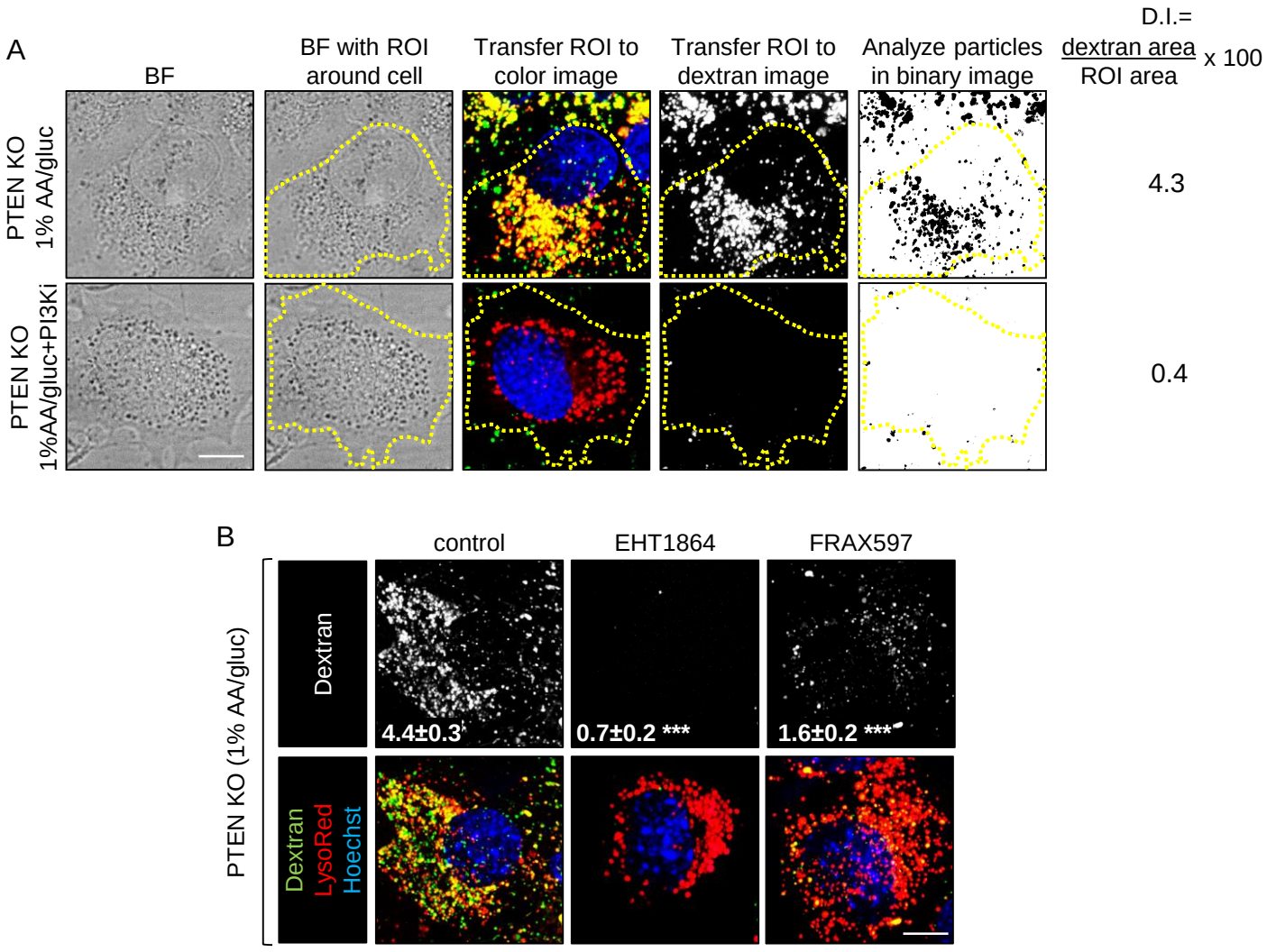

Supplementary Figure S1: PTEN-deficient MEFs exhibit macropinocytosis under nutrient stress, related to Figure 1. **A**) Dextran uptake quantification workflow; see Supplemental Methods for additional information. BF, bright field; ROI, region of interest; D.I., dextran index. **B**) Dextran uptake in PTEN KO MEFs in 1% AA/gluc pre-treated with the RAC1 inhibitor EHT1864 (50 µM) or PAK inhibitor FRAX597 (10 µM) for 1 h. Dextran index in white, means ± SEM shown, statistics relative to control; ≥ 20 cells were examined for each condition.

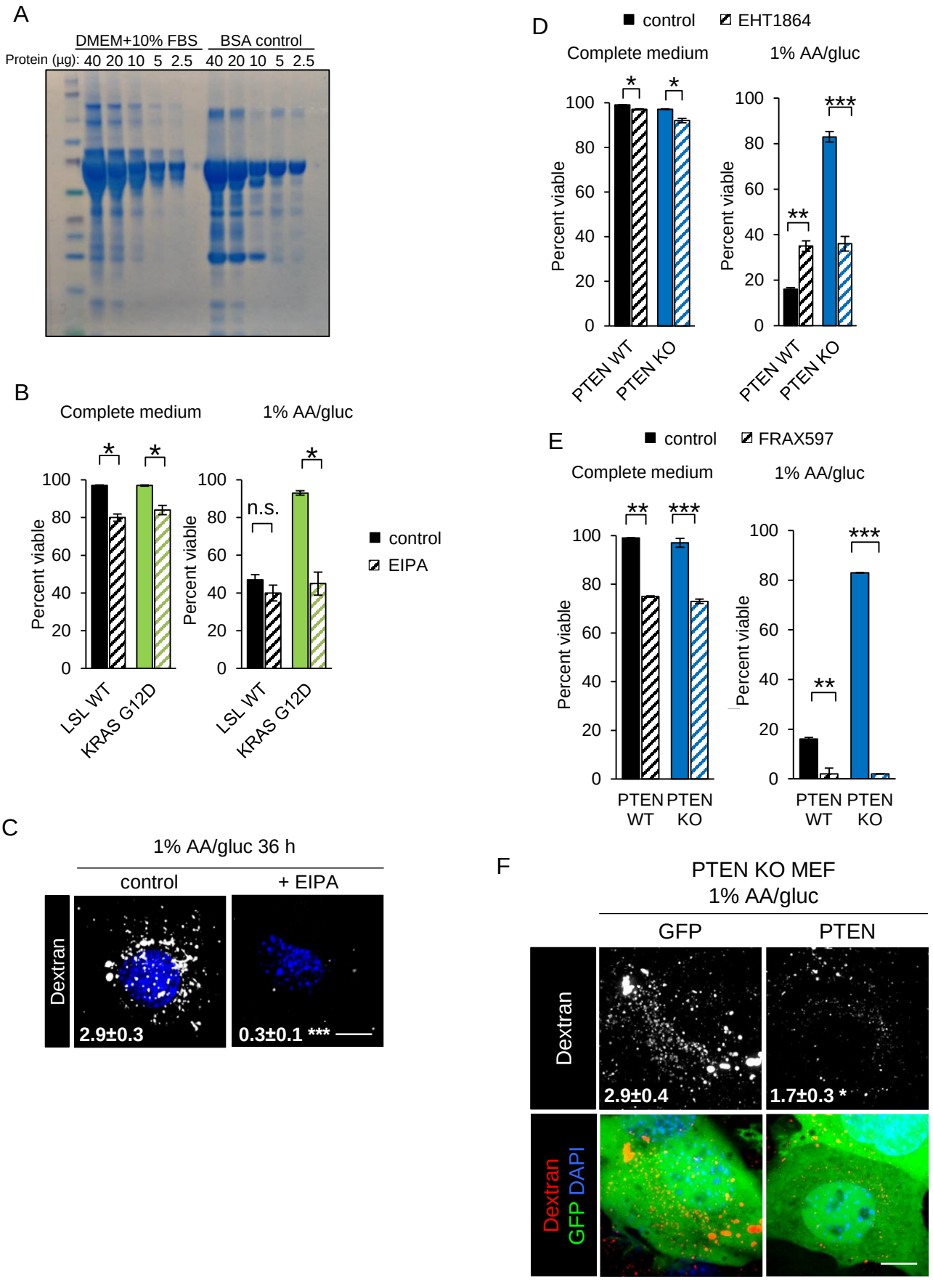

Supplementary Figure S2

Supplementary Figure S2: PTEN-deficient cells use macropinocytosis to consume albumin and survive nutrient stress, related to Figure 1. A) The indicated protein equivalents of complete medium (DMEM with 10% serum) or BSA were evaluated by SDS-PAGE and Coomassie staining. **B**) Viability of LSL WT or KRAS G12D MEF after 48 h in complete medium or 1% AA/gluc ± EIPA (25 µM). **C**) Dextran uptake in PTEN KO MEFs in 1% AA/gluc after 36 h ± EIPA (25 µM). **D,E**) Viability of PTEN WT or KO MEF after 48 h in complete medium or 1% AA/gluc ± EHT1864 (25 µM) (D) or FRAX597 (10 µM) (E). **F**) Dextran uptake in GFP-positive PTEN KO MEFs transfected with GFP or GFP and PTEN in 1% AA/gluc. Scale bars, 20 µm. Dextran index ± SEM indicated in white; statistics relative to control or GFP. n ≥ 3 in panels B**,** D, and E. For imaging ≥ 25 cells were examined. Using a paired, two-tailed t test, *, $P \leq 0.05$; **, $P \leq 0.01$; ***, $P \leq 0.001$, n.s. not significant.

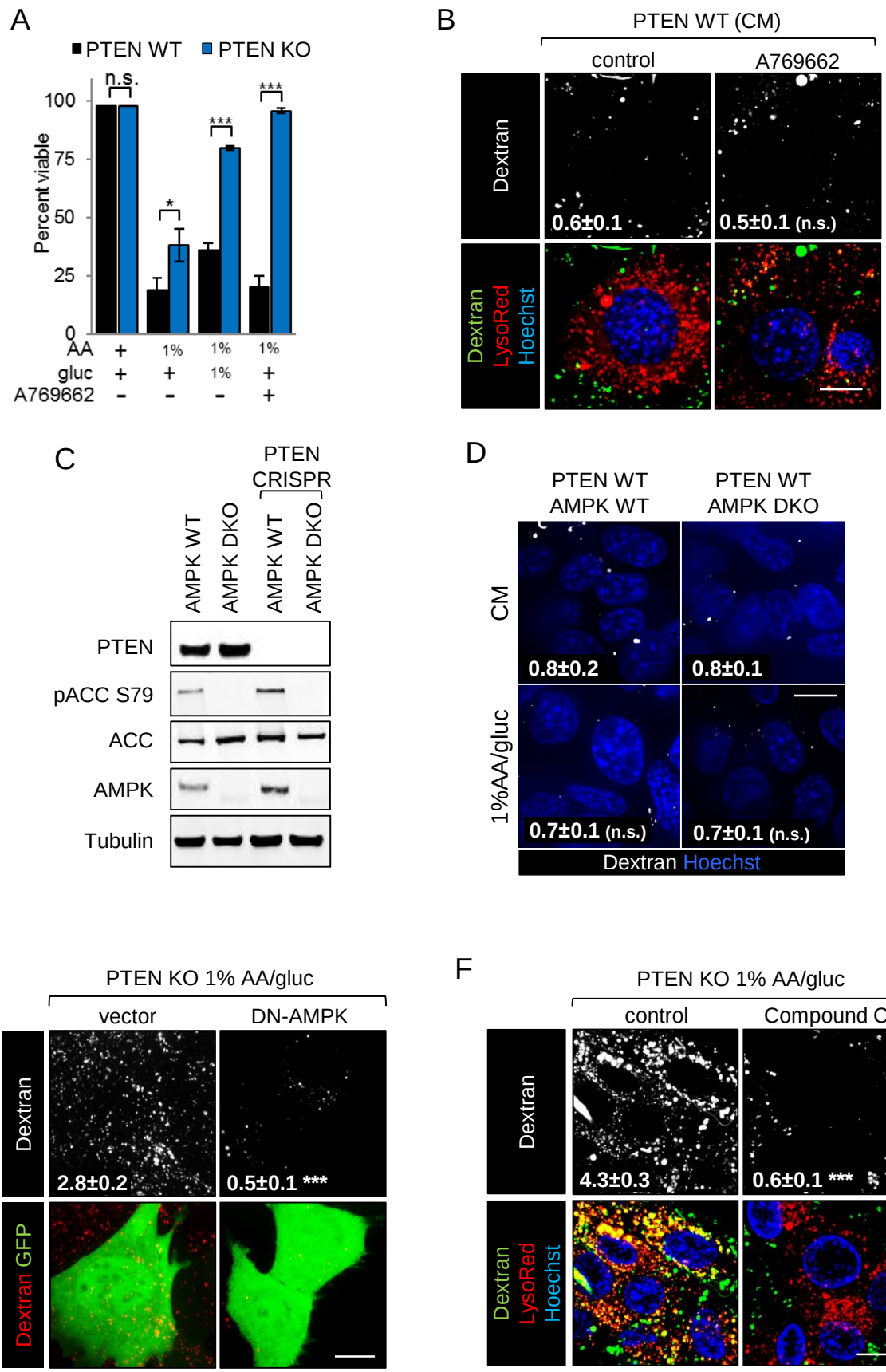

Supplementary Figure S3

Supplementary Figure S3, related to Figure 2. A) Viability of PTEN WT or KO MEFs after 72 h in the indicated media ± A769662 (10 μM). **B**) Dextran uptake in PTEN WT MEFs in CM ± A769662 (50 μM). **C**) Western blot of AMPK WT and DKO MEFs following CRISPR/Cas9-mediated PTEN deletion. **D**) Dextran uptake in AMPK WT or DKO MEFs with WT PTEN in CM or 1% AA/gluc. **E**) Dextran uptake in GFP-positive PTEN KO MEFs expressing GFP or dominant-negative AMPK (DN-AMPK) and GFP in 1% AA/gluc. **F**) Dextran uptake in PTEN KO MEFs in 1% AA/gluc ± Compound C (50 μM). Scale bars, 20 μm. Means ± SEM shown, n ≥ 3 in panel A. Dextran index ± SEM indicated in white; statistics relative to control, CM or vector. For imaging ≥ 25 cells were examined. Using a paired, two-tailed t test, *, $P \leq 0.05$; **, $P \leq 0.01$; ***, $P \leq 0.001$, n.s. not significant.

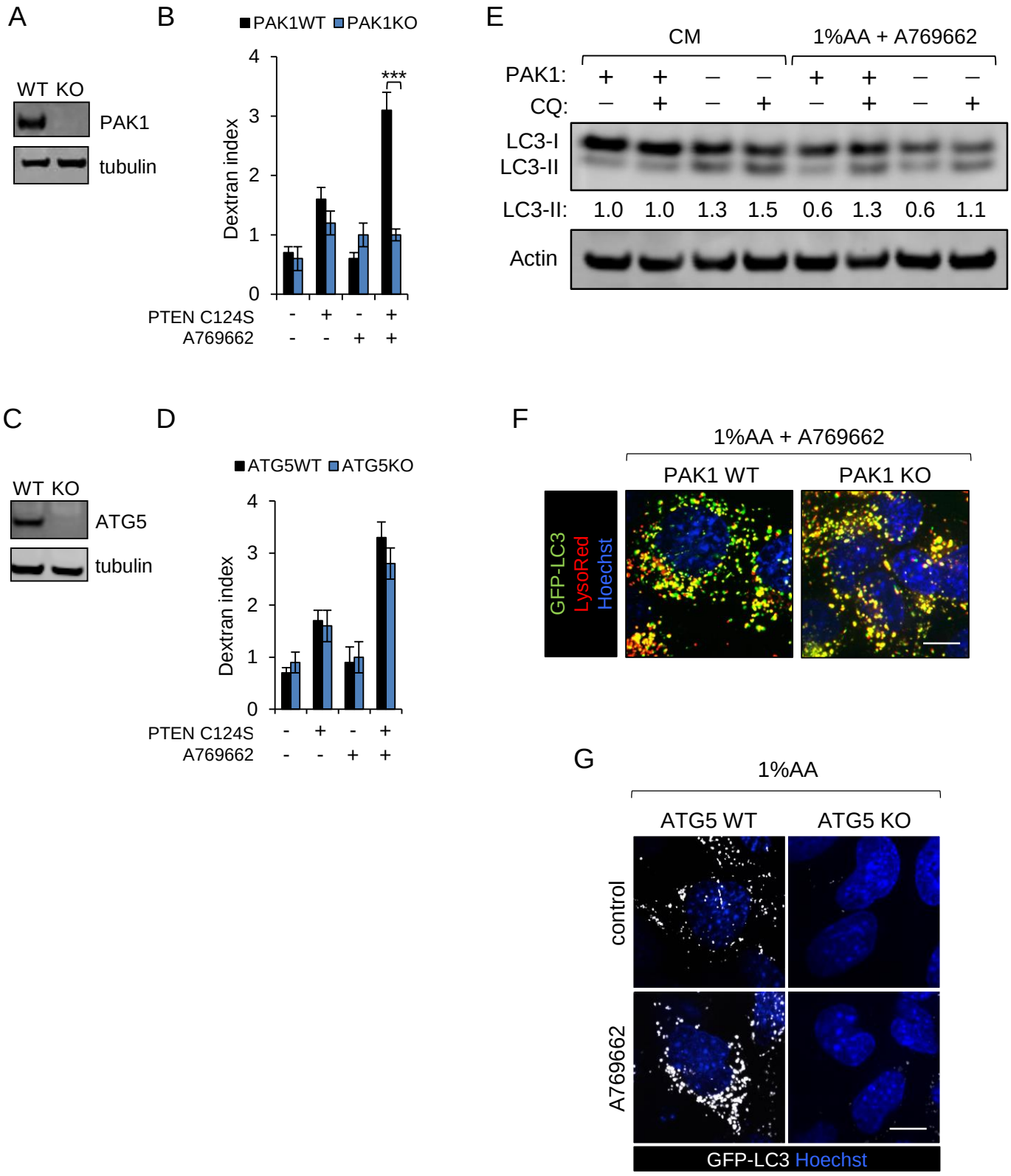

Supplementary Figure S4

Supplementary Figure S4: PAK1 is necessary for macropinocytosis but not autophagy while ATG5 is necessary for autophagy but not macropinocytosis, related to Figure 2. A) Western blot in PAK1 WT and KO MEFs. **B**) Dextran uptake in PAK1 WT or KO MEFs ± PTEN C124S in 1% AA ± A769662 (50 µM). **C**) Western blot in ATG5 WT and KO MEFs. **D**) Dextran uptake in ATG5 WT or KO MEFs ± PTEN C124S in 1% AA ± A769662 (50 µM). **E**) Western blot of PAK1 WT or KO MEFs after 3 h in the indicated medium ± 1.5 h pre-treatment with A769662 (50 µM) ± final 0.5 h incubation with chloroquine (CQ, 50 µM). LC3-II was quantified using LICOR software. **F**) GFP-LC3 and Lysotracker Red in PAK1 WT or KO cells maintained in 1% AA + A769662 (50 µM) for 3 h. **G**) GFP-LC3 in ATG5 WT or KO MEFs maintained in the indicated medium + A769662 (50 µM) for 3 h. Scale bars, 20 µm. In panels B and D, means ± SEM shown, ≥ 25 cells were examined. Using a paired, two-tailed t test, ***, $P \leq 0.001$.

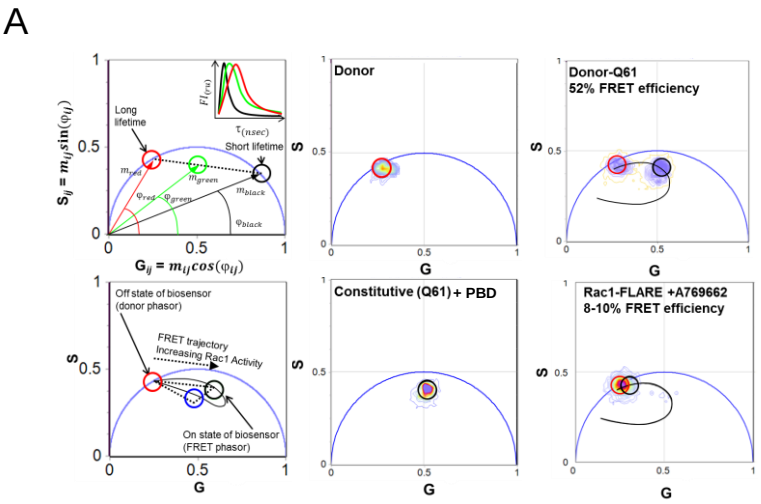

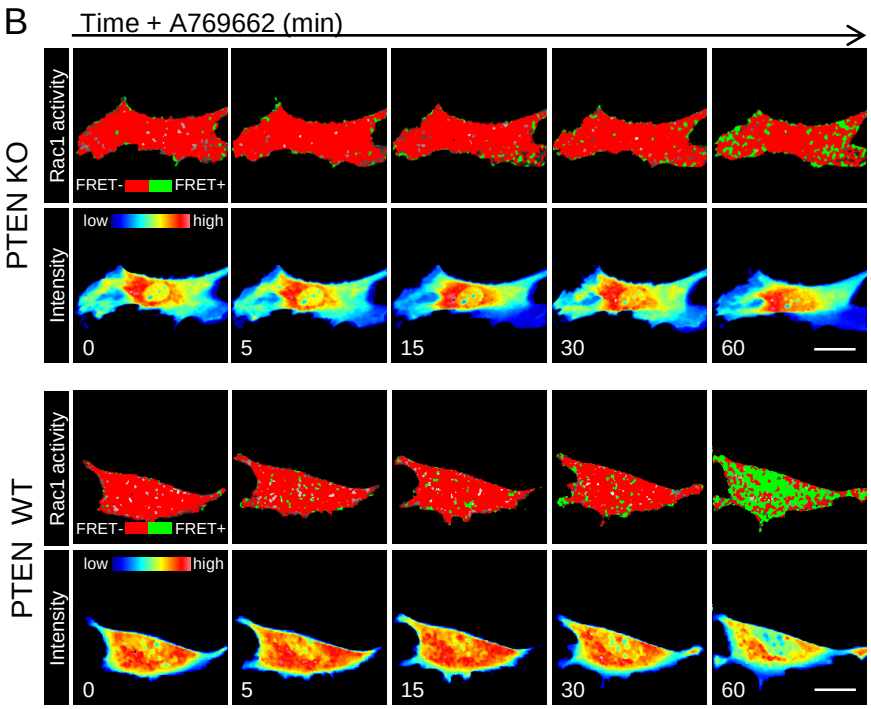

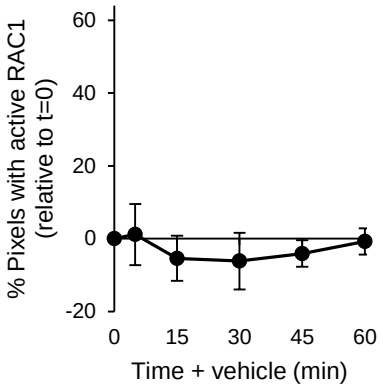

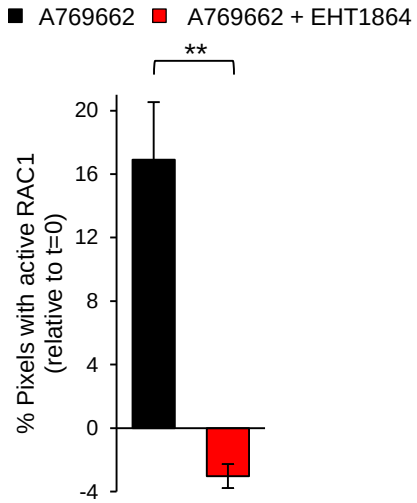

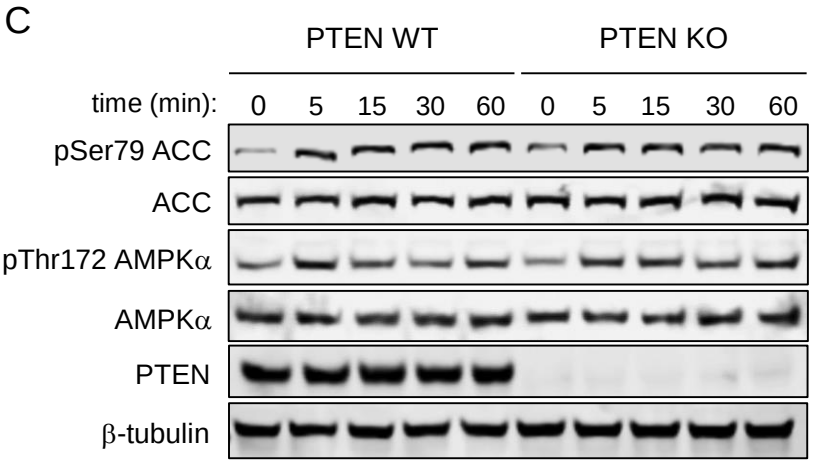

Supplementary Figure S5

Supplementary Figure S5: Analysis of RAC1 biosensor activation by A769662 in MEFs, Related to Figure 2. A) Phasor plot analysis of RAC1 biosensor activity in PTEN KO MEFs. Left top: Phasor plot representation of two simulated fluorescence lifetime decays. Left bottom: FRET analysis represented on the phasor plot. Red cursor indicates the off-state of the inactive RAC1 biosensor (unquenched donor), black cursor indicates maximal on-state of constitutively-active RAC1 biosensor (quenched donor), and blue cursor indicates the position of cellular autofluorescence. From these positions on the phasor plot, the theoretical FRET trajectory of RAC1 biosensor was identified (curved black line). Tracking the FRET trajectory allows for translation of the lifetime shift to FRET efficiency. Middle: Positions of the unquenched donor (top) or quenched donor (bottom) on the phasor plot. Right: FRET efficiency calculated by the trajectory of donor to constitutively-active RAC1 biosensor (top) and FRET efficiency of the RAC1 FLARE biosensor upon the addition of A769662 (bottom). **B**) RAC1 activation in PTEN KO and WT MEFs over time after addition of A769662 (50 µM). Top: Pseudo-color representation of RAC1 activity (FLIM-FRET). Bottom: RAC1 biosensor intensity. The field of view is 74.6 µm x 74.6 µm. Scale bars, 20 µm. **C**) Western blot showing kinetics of AMPK activation in PTEN WT or KO cells treated with A769662 (50 µM). **D**) PTEN KO MEFs were transfected with FLARE RAC1 constructs and imaged by FLIM-FRET. Cells were treated with medium containing DMSO vehicle and imaged at 5, 15, 30, 45, and 60 minutes following addition. The amount of pixels that contain active RAC1 are plotted as a percentage of the total pixels of the cell. (n=3). **E**) PTEN KO MEFs were transfected with FLARE RAC1 constructs and imaged by FLIM-FRET. Following addition of A769662 for 60 minutes, the RAC1 inhibitor EHT1864 was added to block FRET. After 15 minutes with EHT1864 (50 µM), cells were imaged. The amount of pixels that contain active RAC1 are plotted as a percentage of total pixels of the cell. Mean ± SEM shown; **, $P \leq 0.01$ with an unpaired t test (A769662: n=7; A769662 + EHT1864: n=3).

Supplementary Video S1: Spatio-temporal activation of the RAC1 biosensor (GP-FRET) in an A769662-treated PTEN KO MEF. Related to Figure 2. Imaging was performed 2 h after A769662 (50 µM) addition. Color scale for GP-FRET as in Figure 2J. Arrowheads point to macropinosome-like structures.

Supplementary Video S2: RAC1 biosensor (CyPet-RAC1) donor intensity dynamics in an A769662-treated PTEN KO MEF. Related to Figure 2. Imaging was performed 2 h after A769662 (50 µM) addition. Intensity scale as in Figure 2J. Same cell shown as in Figure 2 Supplement Video 1. Arrowheads point to macropinosome-like structures.

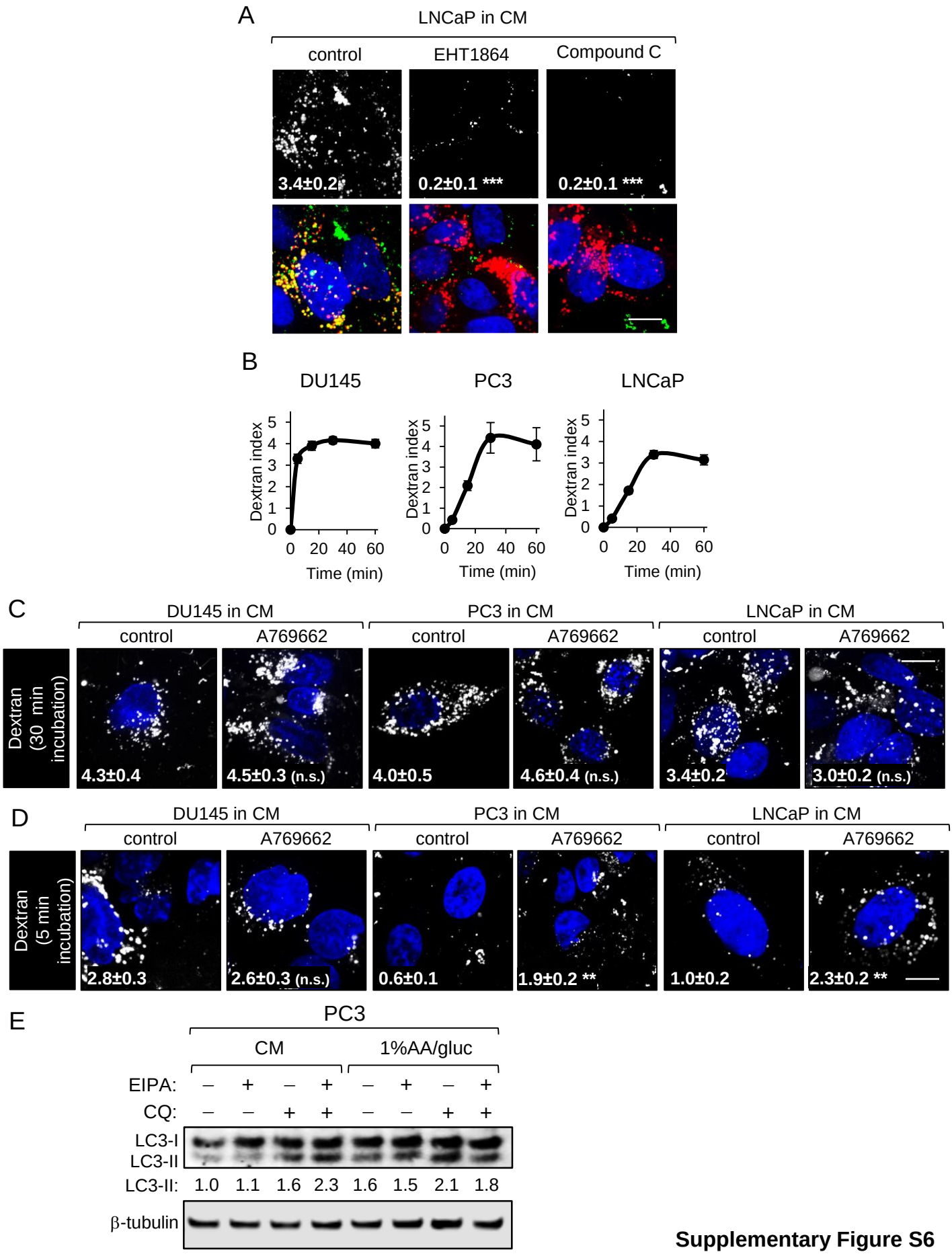

Supplementary Figure S6

Supplementary Figure S6: AMPK promotes macropinocytosis in prostate cancer cells, Related to Figure 4. A) Dextran uptake in LNCaP cells in CM ± pre-treatment (1 h) with EHT1864 (50 µM) or Compound C (50 µM). **B**) Prostate cancer cells were pulsed with dextran for the indicated intervals (0, 5, 15, 30 and 60 min) and dextran uptake quantified. In each cell line, steady state was reached by 30 min. **C,D**) Dextran uptake in prostate cancer cells in complete medium ± A769662 (50 µM) after 30 (C) or 5 (D) min incubation with dextran. Mean ± SEM shown. Scale bars, 20 µm. Dextran index indicated in white in images, mean ± SEM; statistics relative to control, using paired two-tailed t test, **, $P \leq 0.01$; ***, $P \leq 0.001$; n.s., not significant. ≥ 25 cells were examined except for (D) where 15 cells were evaluated. **E**) Western blot of PC3 cells after 1 h in the indicated medium ± chloroquine (CQ, 25 µM). LC3-II was quantified using LICOR software.

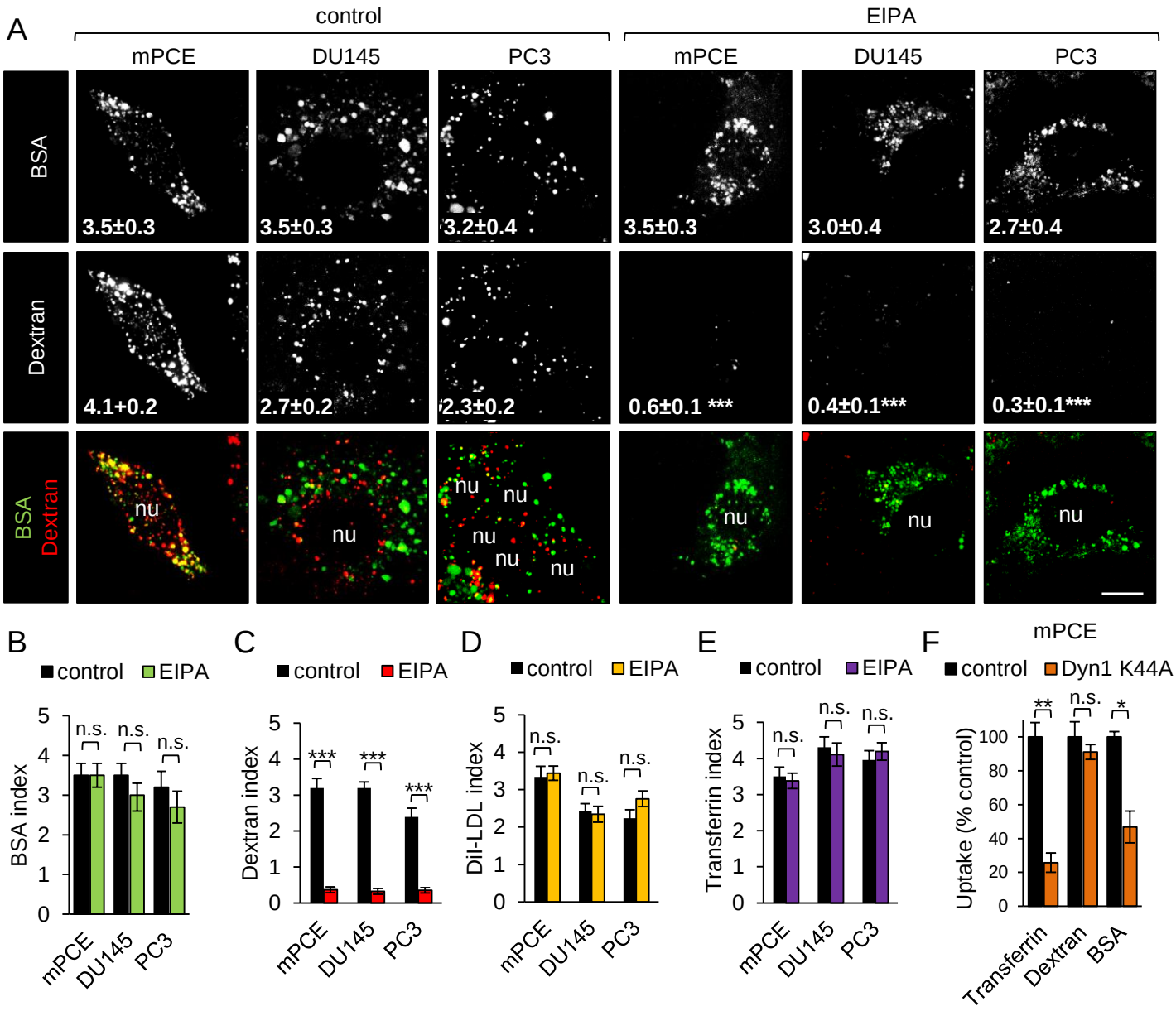

Supplementary Figure S7. BSA uptake in prostate cancer cells is independent of macropinocytosis. A) Alexa 488 BSA or Texas Red dextran uptake in prostate cancer cells ± EIPA (50-75 μM). **B,C**) Quantification of (A). **D**) Dil-LDL uptake ± EIPA (50-75 μM). **E**) Transferrin-488 uptake ± EIPA (50-75 μM). **F**) BSA, dextran, and transferrin uptake in mPCE cells ± DN dynamin1 (Dyn1 K44A). Nu, nucleus. Dextran or BSA Index shown in white. Scale bar 20 μm. Means ± SEM shown, ≥ 15 cells were examined. Using paired two-tailed t test, *, $P \leq 0.05$; **, $P \leq 0.01$; ***, $P \leq 0.001$; n.s., not significant.

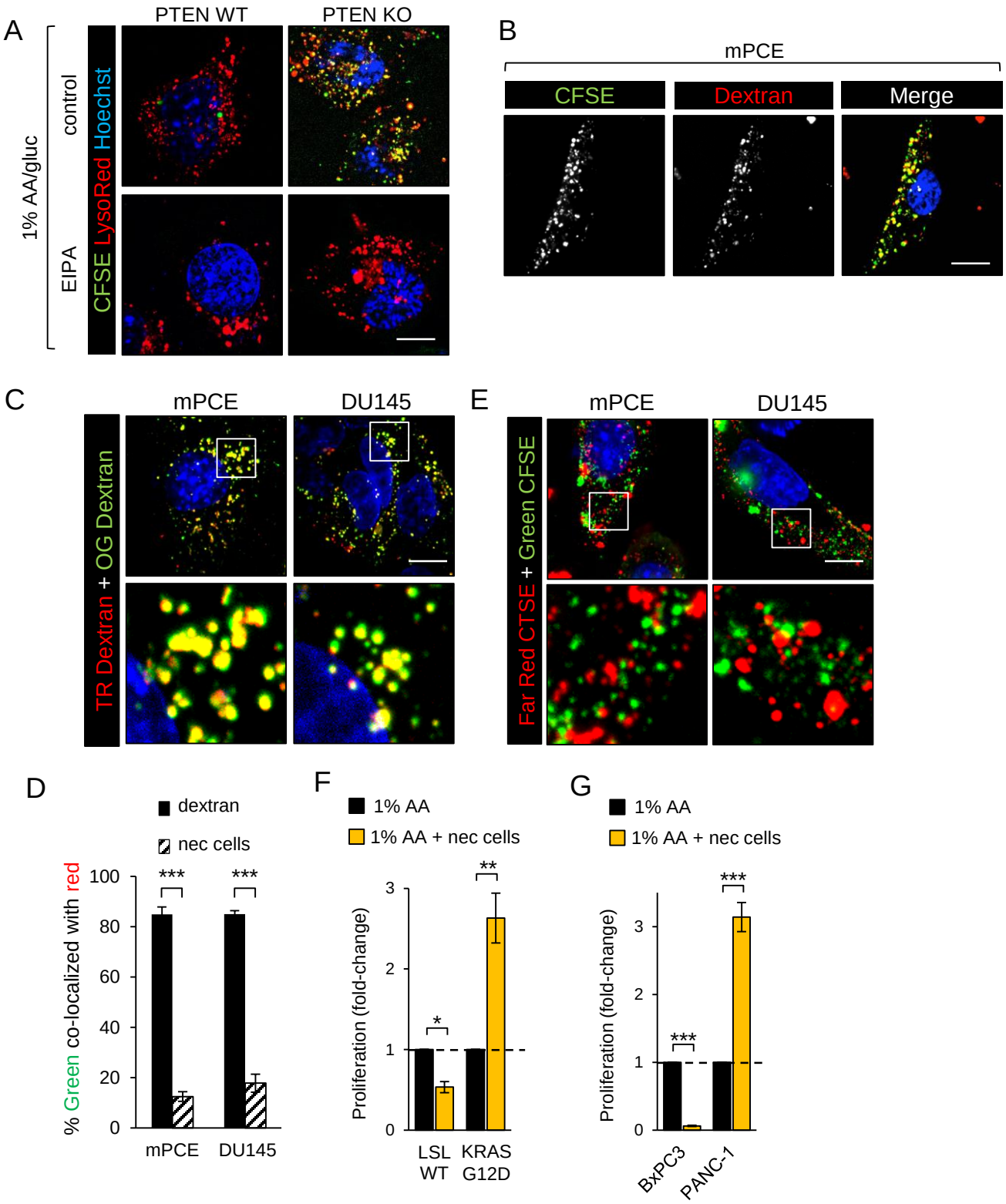

Supplementary Figure S8

Supplementary Figure S8: Necrotic debris is taken up through macropinocytosis in prostate cancer cells, related to Figure 5. A) CFSE-labeled necrotic cell debris uptake in PTEN WT and KO MEFs in 1% AA/gluc ± EIPA (50 µM). **B**) Green CFSE-labeled necrotic cell debris and Texas Red Dextran uptake in mPCE cells in CM. **C**) Texas Red and Oregon Green dextran were added together to mPCE prostate cancer cells in CM and uptake measured after 30 min. **D**) As in (B) except Far Red CTSE- and green CFSE-labeled necrotic cell debris were added instead of dextran. **E**) Quantification of green pixels co-localized with red pixels within cells in (C and D). **F**) Proliferation of control LSL or KRAS G12D MEF after 72 h in 1% AA/gluc ± necrotic debris (0.1% protein). **G**) Proliferation of BxPC3 or PANC-1 cells after 96 h in 1% AA ± necrotic debris (0.1% protein). Scale bars, 20 µm. n ≥ 3 in panels F,G**.** For imaging ≥ 25 cells were examined. Using a paired, two-tailed t test, *, $P \leq 0.05$; **, $P \leq 0.01$; ***, $P \leq 0.001$.

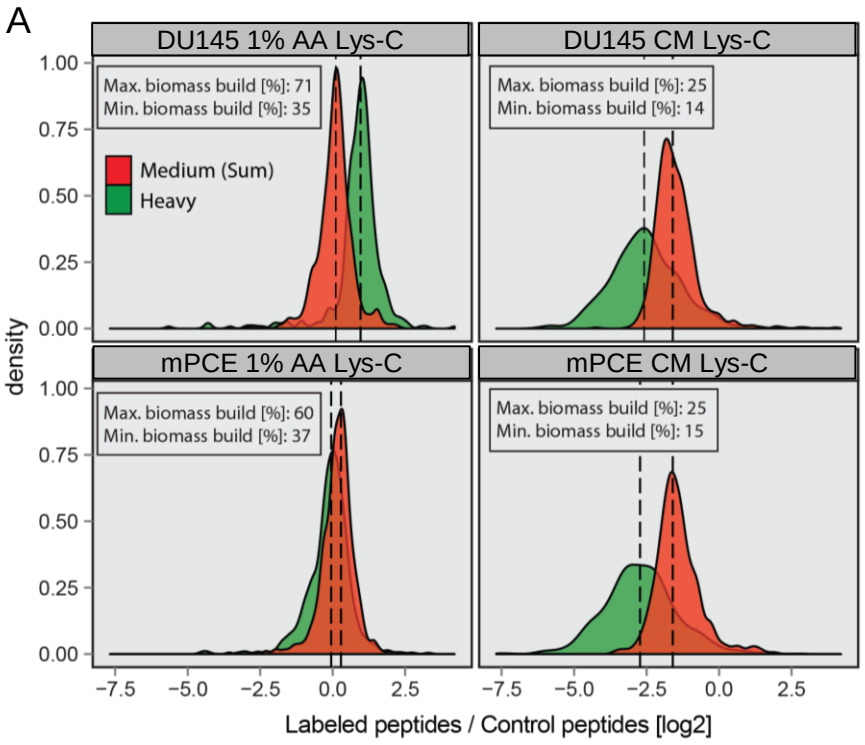

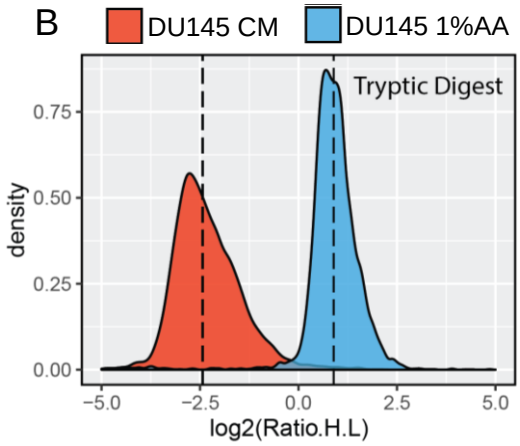

DU145	% newly synthesized biomass, isotopically labeled human protein
1% AA	65%
CM	16%

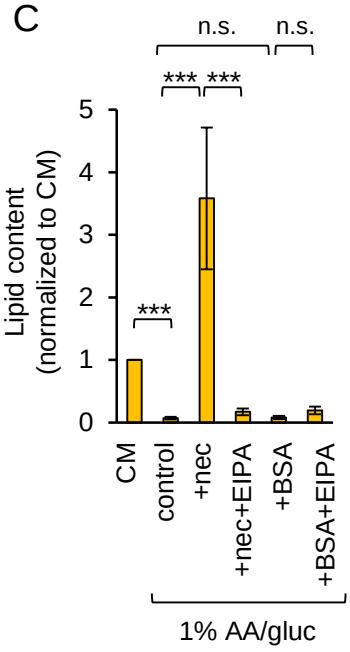

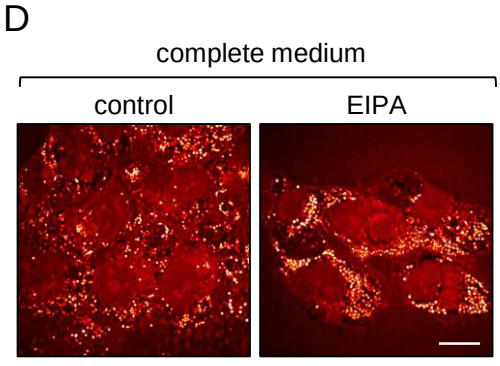

Supplementary Figure S9: Macropinocytosis is used to build biomass, Related to Figure 6. **A**) Measured ratio distributions resulting from Lys-C digests that were used to calculate median biomass in Figures 6D-E. Distribution represents counts versus log2 fold change of peptide ratios measured for medium (red, sum of K4R0 and K0R10 mixed peak ratios) or heavy peptides (green, K4R10) in Lys-C digests. **B**) Tryptic digests of human DU145 cells were used to confirm Lys-C results (Figures 6D-E). Distributions depict SILAC ratios measured in peptides arising from proteins unique to humans in an Andromeda search. The incorporation of isotopically labeled amino acids into 65% of the human peptides in 1% AA medium and 16% in CM is consistent with biomass build estimates using Lys-C digestion. **C**) Quantification of lipid droplets detected by CARS in Figure 6F. **D**) DU145 cells were cultured in complete medium ± 50 μM EIPA for 24 h and fixed with 4% PFA. Lipid droplets were imaged by CARS. ≥ 25 cells were examined. Using a paired, two-tailed t test, *, $P \leq 0.05$; **, $P \leq 0.01$; ***, $P \leq 0.001$, n.s. not significant. Tukey's test was used to correct for multiple comparisons in (C). Scale bar, 20 μm.

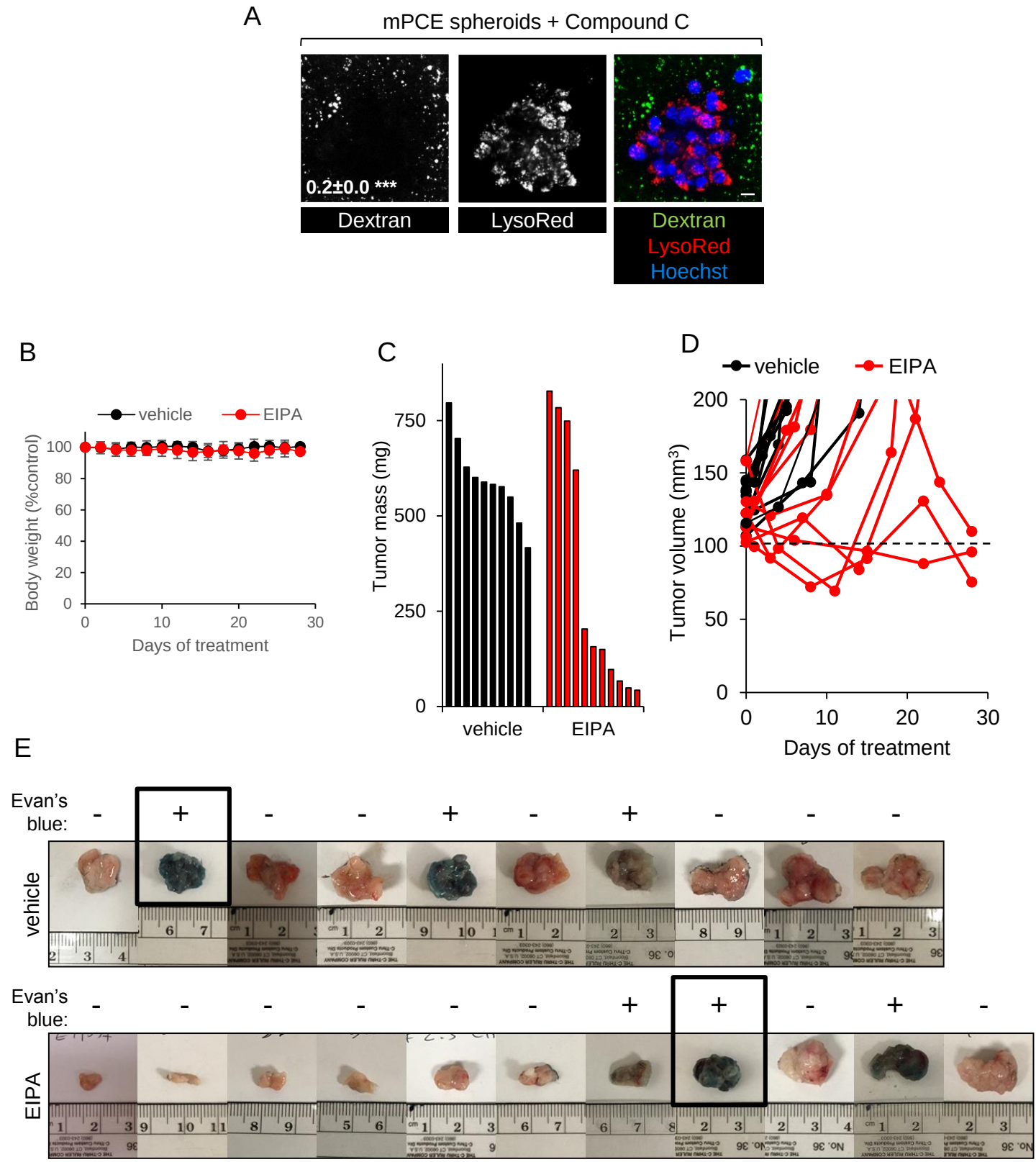

Supplementary Figure S10

Supplementary Figure S10: Inhibiting macropinocytosis reduces prostate tumor growth, Related to Figure 7. A) Dextran uptake in mouse prostate tumor organoids ± Compound C (20 μM). Mean ± SEM shown, statistics relative to control (Fig. 7A). Using a paired two-tailed t test, ***, $P \leq 0.001$. **B-D**) Body weight (B), tumor weight at sacrifice (C), or tumor volume measured with calipers (D) in C57BL/6 mice with subcutaneous mPCE isograft tumors treated with vehicle (1% DMSO in PBS) or EIPA (7.5 mg/kg) subcutaneously every other day once tumors reached 100 mm^3. Panel (D) is the same as Figure 7F but displayed with a Y-axis that allows discrimination of tumor regressions. **E**) mPCE isograft tumors excised from mice in (B-D). Tumors that are blue were from mice intravenously co-injected with FITC-Ficoll and Evan's blue dye prior to sacrifice. Evan's blue dye was used to confirm successful i.v. injection of Ficoll and delivery to tumors even in mice where EIPA blocked tumor cell macropinocytosis. Boxed images indicate tumor samples used in Figure 7H.

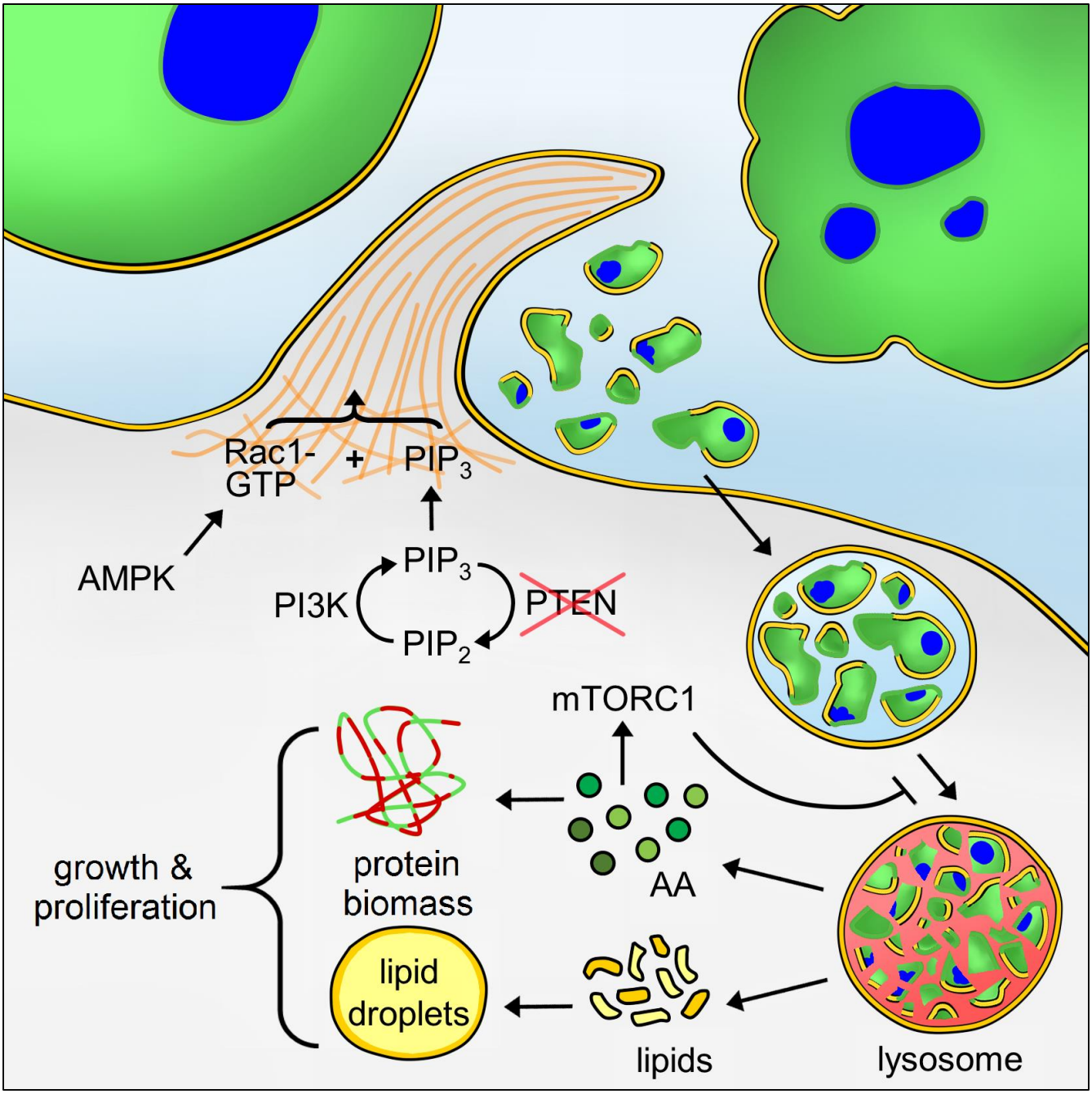

Supplementary Figure S11: Model Figure. PTEN-deficiency induces AMPK-dependent macropinocytosis that allows the conversion of necrotic debris into amino acids and lipids used to drive growth. Intact cells are too large to enter but extracellular proteins may also be engulfed.